INTERNATIONAL JOURNAL OF HYDROGEN ENERGY 35 (2010) 2403–2416

Available at www.sciencedirect.com

ScienceDirect

journal homepage: www.elsevier.com/locate/he

Analysis of liquid water transport in cathode catalyst layer of PEM fuel cells

Prodip K. Das [a,b], *Xianguo Li* [a,*], *Zhong-Sheng Liu* [b]

[a] *Department of Mechanical and Mechatronics Engineering, University of Waterloo, 200 University Avenue West, Waterloo, ON N2L 3G1, Canada*

[b] *Institute for Fuel Cell Innovation, National Research Council, Vancouver, BC V6T 1W5, Canada*

ARTICLE INFO

Article history:
Received 7 August 2009
Accepted 23 December 2009
Available online 25 January 2010

Keywords:
Analytical formulation
Cathode catalyst layer
Liquid water transport
PEM fuel cell
Water flooding

ABSTRACT

The performance of a polymer electrolyte membrane (PEM) fuel cell is significantly affected by liquid water generated at the cathode catalyst layer (CCL) potentially causing water flooding of cathode; while the ionic conductivity of PEM is directly proportional to its water content. Therefore, it is essential to maintain a delicate water balance, which requires a good understanding of the liquid water transport in the PEM fuel cells. In this study, a one-dimensional analytical solution of liquid water transport across the CCL is derived from the fundamental transport equations to investigate the water transport in the CCL of a PEM fuel cell. The effect of CCL wettability on liquid water transport and the effect of excessive liquid water, which is also known as ''flooding'', on reactant transport and cell performance have also been investigated. It has been observed that the wetting characteristic of a CCL plays significant role on the liquid water transport and cell performance. Further, the liquid water saturation in a hydrophilic CCL can be significantly reduced by increasing the surface wettability or lowering the contact angle. Based on a dimensionless time constant analysis, it has been shown that the liquid water production from the phase change process is negligible compared to the production from the electrochemical process.

1. Introduction

Over the last decade, polymer electrolyte membrane (PEM) fuel cells have drawn immense attention as high-efficiency and low-emission power sources, particularly for portable and automotive applications [1]. However, the performance and cost of the PEM fuel cells need to be improved significantly in order to be viable for commercial applications. Among the several key factors that are hindering the PEM fuel cells to be competitive with portable and automotive applications, water management is most crucial [2–9]. The ionic conductivity of PEM is significantly dependent on the membrane hydration. Inadequate membrane hydration results in high electrical resistance as well as the formation of dry and hot spots leading to membrane failure. Conversely, the excessive amount of liquid water in the cathode catalyst layer (CCL), produced from the electrochemical reaction and due to electro-osmotic drag effect, could block the access of reactant gas to the reaction site and lower cell performance. Hence, liquid water is one of the key factors responsible for degradation of electrolyte membrane as well as performance reduction.

Water transport in the CCL of a PEM fuel cell involves several transport and physical processes: (a) electro-osmotic transport of water from the membrane to the CCL, (b) back-diffusion of water from the CCL to the membrane, (c) condensation and evaporation of water, and (d) removal of

* *Corresponding author*. Tel.: +1 519 888 4567x36843; fax: +1 519 885 5862.
E-mail addresses: pkdas@uwaterloo.ca (P.K. Das), x6li@uwaterloo.ca (X. Li), zhong-sheng.liu@nrc-cnrc.gc.ca (Z.-S. Liu).
0360-3199/$ – see front matter
doi:10.1016/j.ijhydene.2009.12.160

liquid water to the gas flow channel through the gas diffusion layer (GDL). The electro-osmotic transport occurs due to the proton transport. Proton migrations drag water along with it from the anode side to the cathode side that can eventually reduce the membrane hydration and block the active reaction site in the CCL. Conversely, the back-diffusion represents the water transport back to the membrane due to the concentration gradient. Since water is produced at the CCL and protons are dragging liquid water from the anode side, the liquid water concentration in the cathode side increases significantly compared to the anode side during the operation of fuel cells. This concentration difference causes diffusion of water from the CCL to the membrane. Further, if the reactant gases are fully humidified, water vapors in the gas mixture tend to condense. Conversely, if the gases are partially hydrated, liquid water will start to saturate the gas mixture through the evaporation process. Furthermore, the liquid water can be removed from the cathode GDL by the flow of reactant gas in the gas flow channel that can eventually dry out the electrode, hence the membrane, if the rate of water removal is too fast. Clearly, the entire water transport process in a PEM fuel cell is a complex phenomenon, hence it is essential to make a delicate water balance for better and optimum fuel cell performance, and prevent material degradation.

There are numerous theoretical and numerical studies related to liquid water transport available in literature [2–4,10–15], however, most of them addressed the liquid water transport in the membrane or the GDL of a PEM fuel cell. These studies also addressed the water flooding in the GDL and gas flow channel, and none of the previous studies specifically addressed the liquid water transport in the CCL of a PEM fuel cell. Further, these studies were based on the assumption that most of the liquid water produced at the GDL/CCL interface or the catalyst layer is very thin. While the highest reaction rate occurs at the membrane/CCL interface [16] and the CCL thickness needs to be higher than 10 μm to obtain optimum performance from a PEM fuel cell [17]. Therefore, the approximation of a thin CCL or considering the CCL as an interface seems to be insufficient to explore the overall liquid water transport in a PEM fuel cell. Substantial amount of experimental studies have also been conducted for the flooding in PEM fuel cells to understand the fundamental water transport processes [5–9,18–20]. Further, Pasaogullari and Wang [21] developed an analytical model of liquid water transport in the GDL of a PEM fuel cell. Although water flooding in the CCL likely occurs prior to that in the flow channel and GDL because of water is produced in the CCL from the electrochemical reaction and is expelled from the CCL to the flow channel through the GDL, the studies related to the CCL flooding are still elusive.

The objective of this study is to investigate liquid water transport in the CCL of a PEM fuel cell. In-situ measurement of water flooding in the CCL is very difficult. Even if possible, for instance, by using NMR Microscopy [22] and Neutron Radiography [18,23], it can only yield a qualitative picture of liquid water distribution in a PEM fuel cell. Therefore, our objective is to provide a simple, easy to implement and quick estimate of liquid water transport in the CCL of a PEM fuel cell. The liquid water transport process has been dealt with analytically, including electro-osmotic transport, back-diffusion, condensation and evaporation of water, and removal of liquid water through GDL. A simplified formulation has been developed from the conservation of mass and momentum equations and the one-dimensional (1D) analytical solutions of liquid water profile have been derived for both hydrophilic and hydrophobic CCLs. Then the effect of catalyst layer wettability and effect of CCL flooding on the performance of a PEM fuel cell have been investigated.

2. The physical problem

In the present study, a typical PEM fuel cell is considered that consists of a cathode and an anode electrode with a proton-conducting membrane as the electrolyte that separates the anode side and the cathode side. Fig. 1 shows a schematic of a PEM fuel cell with key components (left figure) and a cathode catalyst layer with the coordinate system (right

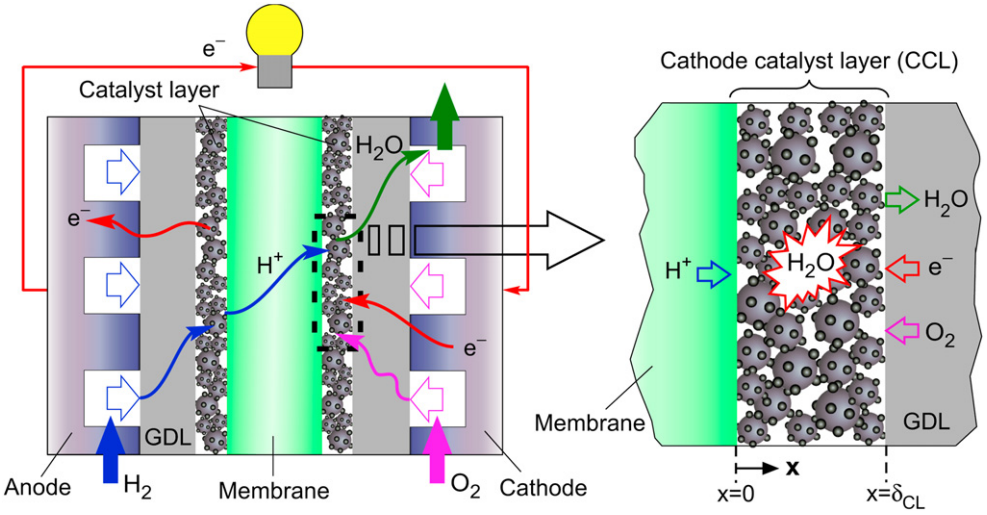

Fig. 1 – The schematic of a PEM fuel cell with key components (left) and a cathode catalyst layer with the coordinate system (right).

figure). In the anode side, humidified H_2 gas is supplied under pressure into the gas flow channel, which diffuses through the porous GDL until it reaches the anode catalyst layer, and dissociates into protons (H^+) and electrons via electro-oxidation reaction at the catalyst surface. The protons are transported through the membrane to the CCL, whereas the electrons are transported via the external circuit to the cathode side that provides electrical energy into the external circuit. Conversely, humidified air is supplied to the cathode gas flow channel, where O_2 (a component of air) diffuses through the GDL until it reaches the CCL and forms water reacting with the proton and electron, as shown in the right-hand part of Fig. 1. The overall electrochemical reaction occurring in a PEM fuel cell can be represented by the following reaction:

$$2H_2 + O_2 \rightarrow 2H_2O + \text{Heat} + \text{Electric Energy} \quad (1)$$

The product water in the CCL needs to be removed to keep the fuel cell operating continuously and to avoid flooding in the CCL and GDL. Water flooding will hinder the reactant transport to the CCL as well as reduce the active reaction area. At the same time, the proton conductivities of the membrane and CCL are highly dependent on its level of hydration. As described in the previous section that the entire liquid water transport process in the CCL is a complex combination of several transport processes, therefore, it is crucial to maintain a delicate water balance. In the present study, we analyze the liquid water transport in the CCL of a PEM fuel cell by addressing several transport processes that are involved in the overall transport process. In the following sections, the conservation equations are described for the liquid water transport in the CCL of a PEM fuel cell and then the governing transport equations are simplified, and analytical solutions are developed for both of the hydrophobic and hydrophilic CCLs.

3. The model development

3.1. *Liquid water transport*

In the CCL of a PEM fuel cell, both the gas and liquid phases co-exist. The liquid phase consists of liquid water only, hence, the transport of liquid water in the CCL of a PEM fuel cell is governed by the microscopic conservation of mass and momentum equations of liquid water phase. To apply the microscopic conservation equations macroscopically, the microscopic equations need to be modified using the volume averaging method. The basic principle of volume averaging procedure for a two-phase flow is to average the single-phase microscopic conservation equations over an elementary volume where several phases co-exist. At steady-state, the volume-averaged conservations equations for liquid phase in the CCL can be written as follows [24]:

$$\nabla\cdot\left(\epsilon_\ell\langle\rho_\ell\rangle^\ell\langle u_\ell\rangle^\ell\right) = \Gamma_{M,\ell} \quad (2)$$

$$\nabla\cdot\left(\epsilon_\ell\langle\rho_\ell\rangle^\ell\langle u_\ell\rangle^\ell\langle u_\ell\rangle^\ell\right) + \nabla\left(\epsilon_\ell\langle P_\ell\rangle^\ell\right) - \langle P_\ell\rangle^\ell\nabla(\epsilon_\ell) - \nabla\cdot\left(\epsilon_\ell\langle t_\ell\rangle^\ell\right) = \Gamma_{F,\ell} \quad (3)$$

where $\langle\rho_\ell\rangle^\ell$ is the phase-averaged density, $\langle u_\ell\rangle^\ell$ is the phase-averaged velocity, $\langle\rho_\ell\rangle^\ell$ is the phase-averaged pressure, and $\langle\tau_\ell\rangle^\ell$ is the phase-averaged viscous stress tensor in the liquid phase of a two-phase mixture in the CCL. The source terms for the conservation of mass and momentum equations are represented by $\Gamma_{M,\ell}$ and $\Gamma_{F,\ell}$, respectively. The term, ϵ_ℓ, represents the volume fraction of liquid water over the elementary volume, that will relate a volume-averaged quantity ($\langle\Psi_\ell\rangle$) to a phase-averaged quantity ($\langle\Psi_\ell\rangle^\ell$) through the following relation:

$$\epsilon_\ell = \frac{\langle\Psi_\ell\rangle}{\langle\Psi_\ell\rangle^\ell} \quad (4)$$

It should be pointed out that in Eqs. (2)–(4) the subscript ℓ represents the phase where the quantity is being estimated and the superscript ℓ represents the phase where the quantity is being averaged. In the porous CCL with the liquid and gas phases, the volume fraction for each phase can be related to the porosity of the medium as

$$\epsilon_l + \epsilon_g = \epsilon \quad (5)$$

where ϵ_l and ϵ_g are the volume fractions of liquid and gas phases, respectively, and ϵ is the porosity.

Assuming the production of water in the CCL from the electrochemical reaction is in liquid form, the source term for the conservation of mass equation can be written as

$$\Gamma_{M,\ell} = \hat{M}_{H_2O}A_v\dot{\mathscr{P}}^{H_2O} + A\left(x_g^{H_2O}\langle P_g\rangle^g - P_{sat}\right) \quad (6)$$

where the first term in the right-hand side represents the production from the electrochemical reaction and the second term represents the production/consumption due to the phase change. In Eq. (6), $\hat{M}_{H_2O}$ is the molecular weight of water, A_v is the catalyst reactive surface area per unit volume, $\dot{\mathscr{P}}^{H_2O}$ is the molar production of liquid water from the electrochemical reaction, A is the interfacial mass-transfer rate between the gas and liquid phases, $x_g^{H_2O}$ is the mole fraction of water vapor, $\langle P_g\rangle^g$ is the phase-averaged gas phase pressure, and P_{sat} is the saturation pressure of water at operating temperature. The specific reaction surface area (A_v) can be estimated from the catalyst mass loading per unit area of cathode (m_{Pt}), catalyst surface area per unit mass of the catalyst (A_s), and catalyst layer thickness (δ_{CL}) as follows [17]:

$$A_v = \frac{A_s m_{Pt}}{\delta_{CL}} \quad (7)$$

The interfacial mass-transfer rate can be estimated from [15]

$$A = k_c\frac{\epsilon(1-s_\ell)x_g^{H_2O}\hat{M}_{H_2O}}{\mathscr{R}T} + k_v\epsilon s_\ell\langle\rho_\ell\rangle^\ell \quad (8)$$

where the first term in the right-hand side represents the condensation rate and the second term represents the evaporation rate. Equation (8) basically assumes that the interfacial mass-transfer rate is proportional to the amount of reactant in the porous media and the driving force, the difference between water partial pressure and its saturation pressure. Here k_c and k_v are the rate constants for condensation and vaporization, respectively. The term, s_ℓ, represents the liquid water saturation, $\mathscr{R}$ is the universal gas constant, and T is the operating temperature.

The source term for the conservation of momentum equation in the CCL is:

$$\Gamma_{F,\ell} = -\frac{\epsilon_\ell \mu_\ell}{K k_{r\ell}} \langle u_\ell \rangle^\ell \tag{9}$$

where μ_ℓ is the liquid water viscosity, K is the permeability, and $k_{r\ell}$ denotes the relative permeability of the liquid phase in the CCL. The phase relative permeability is the ratio of the intrinsic permeability for the phase at a given saturation to the total intrinsic permeability of a porous medium. Physically, the relative permeability of a phase describes the extent to which one phase is hindered by other in pore spaces, and hence can be formulated as a function of liquid water volume fraction (i.e. liquid water saturation). The simplest approach is to consider the relative permeability as a linear function of saturation [25], while the cubic relation is most widely used that can be represented by the following empirical correlation [26]:

$$k_{r\ell} = s_\ell^3 \tag{10}$$

where s_ℓ is the liquid water saturation. Since the liquid phase consists of liquid water only, the term s_ℓ can be simply referred to as liquid saturation. The relative permeability is also a function of capillary pressure, P_c, which is the difference between the gas and liquid phase pressures, i.e.,

$$P_c = P_g - P_\ell \tag{11}$$

For the two-phase flow in a porous CCL, the capillary pressure can be modeled by the following empirical correlation [27]:

$$P_c = \gamma \cos\theta_c \left(\frac{\epsilon}{K}\right)^{0.5} F(s_\ell) \tag{12}$$

where γ is the surface tension between the gas and liquid phases and θ_c is the contact angle. The term $F(s_\ell)$ is the Leverett function that represents the dimensionless capillary pressure as a function of liquid saturation. For the hydrophilic ($\theta_c < 90^\circ$) and hydrophobic ($\theta_c > 90^\circ$) CCLs, the Leverett functions are given by the following relations [21,27,28]:

$$F(s_\ell) = \begin{cases} 1.417(1-s_\ell) - 2.120(1-s_\ell)^2 + 1.263(1-s_\ell)^3 & \text{if } \theta_c < 90^\circ \\ 1.417 s_\ell - 2.120 s_\ell^2 + 1.263 s_\ell^3 & \text{if } \theta_c > 90^\circ \end{cases} \tag{13}$$

In a hydrophilic medium, the wetting phase is the liquid phase and in a hydrophobic medium, the wetting phase is the gas phase. Hence, the Leverett functions are expressed by the gas phase saturation, $(1 - s_\ell)$, and liquid phase saturation, s_ℓ, respectively. Several other correlations are also available in the literature that relate the liquid saturation in fuel cell to the capillary pressure [29–31], while the Leverett function has been widely used in fuel cell studies. In addition, Pasaogullari and Wang [21] developed the analytical model for liquid water transport in the GDL of a PEM cell using the Leverett function. Hence for the liquid water transport in CCL, the Leverett function is considered for consistency.

3.2. Electrochemical reaction rate

The electrochemical reaction occurring in the CCL of a PEM fuel cell is the oxygen reduction reaction that can be represented by the following reaction:

$$O_2 + 4H^+ + 4e^- \rightleftharpoons 2H_2O \tag{14}$$

The rate of reaction for the above-mentioned chemical reaction in mol m^{-2} s^{-1} can be represented by the Butler–Volmer equation as [1]

$$\mathscr{R}_{c,\mathrm{red}} = \frac{J_0^{O_2}}{n\mathscr{F}} \left[\frac{C_{O_2,\mathrm{rs}}}{C_{O_2,\mathrm{ref}}}\right] \left\{ \exp\left(\frac{n\alpha_a \mathscr{F} \eta_c}{\mathscr{R}T}\right) - \exp\left(-\frac{n\alpha_c \mathscr{F} \eta_c}{\mathscr{R}T}\right) \right\} \tag{15}$$

where $J_0^{O_2}$ is the reference exchange current density for oxygen reduction reaction, $\mathscr{F}$ is the Faraday's constant (96487 C mol^{-1}), $\mathscr{R}$ is the universal gas constant (8.315 J mol^{-1} K^{-1}), $C_{O_2,\mathrm{rs}}$ and $C_{O_2,\mathrm{ref}}$ are the oxygen concentration at the reaction site and reference oxygen concentration, respectively. The terms, α_a and α_c, are the apparent transfer coefficients for the anodic and cathodic reactions, respectively, n is the number of electrons transferred in the electrochemical reaction, and η_c represents the activation overpotential, which is the driving force for the electrochemical reaction. The reference exchange current density, $J_0^{O_2}$, in A cm^{-2} for oxygen reduction corresponding to the low Tafel slope (about −70 mV $decade^{-1}$) at the Pt/Nafion interface is correlated with the cell temperature based on the experimental data of Parthasarathy et al. [32] with a confidence level of 97.72% as

$$\log_{10}\left(J_0^{O_2}\right) = 3.504 - \frac{4001.135}{T} \tag{16}$$

where T is the temperature in Kelvin. Based on the electrochemical reaction and the rate of reaction given in Eqs. (14) and (15), the molar production of liquid water in the CCL of a PEM fuel cell, in unit of mol m^{-2} s^{-1}, can be written as

$$\dot{\mathscr{P}}^{H_2O} = 2\mathscr{R}_{c,\mathrm{red}} \tag{17}$$

3.3. One-dimensional liquid water transport

The liquid water transport inside the CCL of a PEM fuel cell is mainly driven by the liquid pressure gradient according to the Darcy's law. Hence, the conservation of momentum equation for the liquid phase can be simplified by neglecting the convective and viscous terms for the steady-state case as

$$\epsilon_\ell \nabla \langle P_\ell \rangle^\ell = -\frac{\epsilon_\ell \mu_\ell}{K k_{r\ell}} \langle u_\ell \rangle^\ell \tag{18}$$

Substituting Eq. (11) in Eq. (18) yields

$$-\nabla P_c + \nabla \langle P_g \rangle^g = -\frac{\mu_\ell}{K k_{r\ell}} \langle \mathbf{u}_\ell \rangle^\ell \tag{19}$$

The gas phase pressure can be considered constant throughout the CCL and GDL of a PEM fuel cell, and is equal to the gas phase pressure in the cathode flow channel [21]. Assuming a constant gas phase pressure and solving Eq. (19) for $\langle \mathbf{u}_\ell \rangle^\ell$ and substituting into Eq. (2) yields

$$\nabla \cdot \left(\frac{K k_{r\ell}}{\mu_\ell} \langle \rho_\ell \rangle \frac{dP_c}{ds_\ell} \nabla s_\ell \right) = \Gamma_{M,\ell} \tag{20}$$

Considering the one-dimensional transport of liquid water in the through-plane direction of catalyst layer, Eq. (20) reduces to an ordinary differential equation that can be solved analytically with appropriate approximation and boundary conditions.

Assuming the reactant gas is fully humidified, the evaporation part from Eq. (8) can be neglected and hence, the right-hand part of Eq. (20) reduces to

$$\Gamma_{M,\ell} = \hat{M}_{H_2O} A_v \dot{\mathscr{P}}^{H_2O} + k_c \frac{\epsilon x_g^{H_2O} \hat{M}_{H_2O}}{\mathscr{R}T}\left(x_g^{H_2O}\langle P_g\rangle^g - P_{sat}\right) \quad (21)$$

The molar production of liquid water, $\dot{\mathscr{P}}^{H_2O}$, is the function of reaction rate and hence, oxygen concentration and activation overpotential. Later in Sections (3.5) and (3.6), we describe how these quantities are evaluated in the CCL of a PEM fuel cell.

After integrating Eq. (20) with respect to x yields

$$\frac{Kk_{r\ell}}{\mu_\ell}\langle\rho_\ell\rangle\frac{dP_c}{ds_\ell}\nabla s_\ell = x\Gamma_{M,\ell} + C_1 \quad (22)$$

where C_1 is the integration constant. The boundary condition for Eq. (22) at the membrane/CCL interface can be written as

$$\left[\frac{Kk_{r\ell}}{\mu_\ell}\langle\rho_\ell\rangle\frac{dP_c}{ds_\ell}\nabla s_\ell\right]\Big|_{x=0} = 2\alpha\left(\frac{J}{2\mathscr{F}}\hat{M}_{H_2O}\right) \quad (23)$$

where α is the net drag coefficient, J is the current density, $\mathscr{F}$ is the Faraday's constant, and $\hat{M}_{H_2O}$ is the molar mass of water. The net drag coefficient includes both electro-osmotic drag and back-diffusion between the membrane and CCL. Hence, the right-hand side term in Eq. (23) describes the overall water transport through the membrane to the CCL [33,34]. The coefficient, α, is positive when water transport by the electro-osmotic drag is higher than the back-diffusion from the CCL to the membrane, and will be negative when water transport by the electro-osmotic process is lower than the back-diffusion process. If water transport by the electro-osmotic drag is equal to the back-diffusion, then one can assume that the net transport of water across the membrane is zero. Using the boundary condition given in Eq. (23), the first integration constant is found as

$$C_1 = 2\alpha\left(\frac{J}{2F}\hat{M}_{H_2O}\right) \quad (24)$$

The volume-averaged liquid water density, $\langle\rho_\ell\rangle$, can be written in terms of phase-averaged density as

$$\langle\rho_\ell\rangle = \epsilon s_\ell \langle\rho_\ell\rangle^\ell = \epsilon s_\ell \rho_\ell \quad (25)$$

Hence, using the Leverett function, Eq. (22) simplifies in terms of liquid saturation for a hydrophilic CCL ($\theta_c < 90^\circ$) as

$$s_\ell^4\left(-0.966 + 3.338s_\ell - 3.789s_\ell^2\right)\frac{ds_\ell}{dx} = xR_w + R_d \quad (26)$$

and for a hydrophobic CCL ($\theta_c > 90^\circ$) as

$$s_\ell^4\left(1.417 - 4.240s_\ell + 3.789s_\ell^2\right)\frac{ds_\ell}{dx} = xR_w + R_d \quad (27)$$

The terms, R_w and R_d, are represented by the following expressions:

$$R_w = \frac{\nu_\ell}{\epsilon(\epsilon K)^{0.5}\gamma\cos\theta_c}\left[2\hat{M}_{H_2O}A_v\mathscr{R}_{c,red} + k_c\frac{\epsilon x_g^{H_2O}\hat{M}_{H_2O}}{\mathscr{R}T}\left(x_g^{H_2O}\langle P_g\rangle^g - P_{sat}\right)\right] \quad (28)$$

$$R_d = \frac{\nu_\ell}{\epsilon(\epsilon K)^{0.5}\gamma\cos\theta_c}\left[\frac{\alpha\hat{M}_{H_2O}J}{\mathscr{F}}\right] \quad (29)$$

where ν_ℓ is the kinematic viscosity of liquid water. After integrating Eqs. (26) and (27), the liquid saturation expressions have been obtained for a hydrophilic CCL as

$$-0.541s_\ell^7 + 0.556s_\ell^6 - 0.193s_\ell^5 = 0.5x^2R_w + xR_d + C_{21} \quad (30)$$

and for a hydrophobic CCL as

$$-0.541s_\ell^7 + 0.707s_\ell^6 - 0.28s_\ell^5 = 0.5x^2R_w + xR_d + C_{22} \quad (31)$$

where C_{21} and C_{22} are the second integration constants that are governed by the second boundary condition, which is the liquid saturation at the GDL/CCL interface of a PEM fuel cell. Once the liquid saturation at the GDL/CCL interface is known, C_{21} and C_{22} can easily be calculated. In addition, the terms, R_w and R_d, in the liquid saturation expressions are the functions of reaction rate and current density, respectively. Hence, it is possible to relate liquid saturation with the cathode activation overpotential that will eventually allow us to study the effect of liquid saturation on the PEM fuel cell performance. In the following subsections, the boundary condition at the GDL/CCL interface is derived from the formulation proposed by Pasaogullari and Wang [21], followed by the estimation of oxygen concentration at the reaction site and activation overpotential in the CCL of a PEM fuel cell that are based on our earlier study [17].

3.4. *Boundary condition for GDL/CCL interface*

The boundary condition at the GDL/CCL interface can be defined as

$$s_\ell|_{x=\delta_{CL}} = s_b \quad (32)$$

where s_b is a known liquid saturation at the GDL/CCL interface. To estimate s_b, we employed the analytical formulation developed by Pasaogullari and Wang [21] for the liquid water transport in the GDL of a PEM fuel cell. Using the formulation of Pasaogullari and Wang [21], the following expressions are derived:

$$s_b^4\left(0.354 - 0.848s_b + 0.613s_b^2\right) = -\frac{J}{2\mathscr{F}}\hat{M}_{H_2O}\frac{\nu_\ell\delta_{GDL}}{(\epsilon K)^{0.5}\gamma\cos\theta_c} \text{ for } \theta_c > 90^\circ \quad (33)$$

$$s_b^4\left(-0.241 + 0.668s_b - 0.613s_b^2\right) = -\frac{J}{2\mathscr{F}}\hat{M}_{H_2O}\frac{\nu_\ell\delta_{GDL}}{(\epsilon K)^{0.5}\gamma\cos\theta_c} \text{ for } \theta_c < 90^\circ \quad (34)$$

where δ_{GDL} is the GDL thickness.

It should be noted here, for simplicity, Pasaogullari and Wang [21] assumed that no liquid saturation is present in the gas flow channel. However, it is possible to consider a liquid saturation in the flow channel; in such case, the formulation of Pasaogullari and Wang [21] needs to be re-derived to obtain the boundary value (s_b) of liquid saturation. It has also been assumed in Ref. [21] that the net transport of water across the membrane is zero. Since the objective of this study is to use the formulation given in Ref. [21] to obtain the boundary condition at the GDL/CCL interface, no changes have been made to the above-mentioned assumptions. The variations of

liquid saturation at the GDL/CCL interface (s_b) with the current density for GDLs having contact angles of 80° and 100° are shown in Fig. 2. These results are plotted using the expressions given in Eqs. (33) and (34). The results show that the liquid saturation at the GDL/CCL interface for a current density of 1.4 A cm^{-2} would be about 11% higher for a GDL having contact angle of 80° compared to a GDL having contact angle of 100°. Hence, the liquid water removal rate will be higher for a hydrophobic GDL than a hydrophilic GDL. Therefore, in this study only hydrophobic GDL is considered while investigating the liquid water transport in the CCLs of PEM fuel cells.

3.5. Oxygen concentration at reaction site

In order to estimate the oxygen concentration at the reaction site, we employed the mathematical formulation derived earlier. The details of this formulation can be found elsewhere [17], here only few key steps are mentioned. During the transport process in the cathode gas flow channel, oxygen first convects to the GDL surface, and then diffuses through the GDL to the CCL. Considering an uniform oxygen concentration in the cathode flow channel ($C_{O_2,ch}$), the average concentration at the GDL surface ($C_{O_2,gs}$) can be defined as a function of current density by [17]

$$C_{O_2,gs} = C_{O_2,ch} - \frac{J}{4\mathscr{F}} \frac{d_h WL}{ShA_{ch}D_{O_2,bulk}} \tag{35}$$

where d_h is the hydraulic diameter of flow channel, W is the cell width, L is the cell length, $D_{O_2,bulk}$ is the oxygen diffusion coefficient in the gas mixture in flow channel, and A_{ch} is the flow channel area exposed to the GDL. The Sherwood number is denoted by Sh, and due to the laminar flow in the flow channel, is equal to 2.3. The bulk oxygen diffusion coefficient is calculated according to [35]

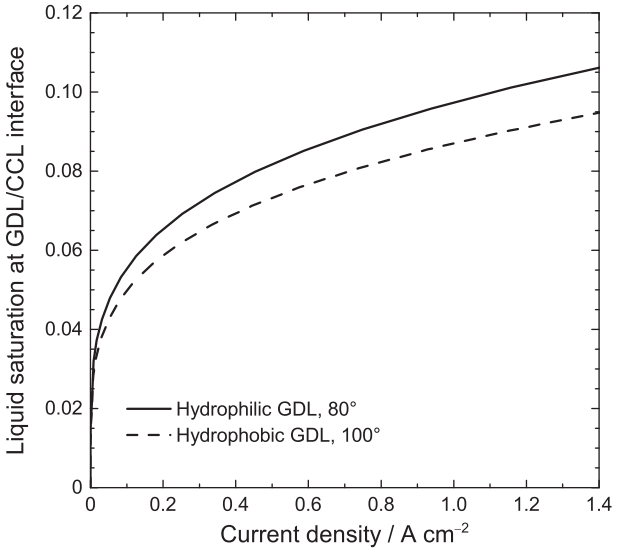

Fig. 2 – Liquid saturation at the GDL/CCL interface of a PEM fuel cell as a function of current density for GDLs having contact angles of 80° and 100° as indicated in the legend.

$$D_{O_2,bulk} = \frac{1 - x_{O_2}}{\frac{x_{N_2}}{D_{O_2-N_2}} + \frac{x_{H_2O}}{D_{O_2-H_2O}}} \tag{36}$$

where x_{O_2}, x_{N_2}, and x_{H_2O} are the mole fractions of oxygen, nitrogen, and water vapor in the gas flow channel, respectively. The binary diffusion coefficient of oxygen and nitrogen, $D_{O_2-N_2}$, can be estimated using the Chapman-Enskog formula [35], while the binary diffusion coefficient of oxygen and water vapor, $D_{O_2-H_2O}$, can be calculated using the Slattery–Bird equation [36]. Once the concentration on the electrode surface is known, the oxygen concentration at the reaction site can be estimated as

$$C_{O_2,rs} = C_{O_2,gs} - N''_{O_2} R_{GDL} \tag{37}$$

in which R_{GDL} is the resistance to mass transfer caused by the oxygen diffusion through the GDL, and N''_{O_2} is the molar flux of oxygen from the gas flow channel to the reaction site in CCL. In the above equation, the mass transport resistance from the CCL/GDL interface to the reaction site is assumed to be negligible compared to the mass transport resistance from the flow channel to the CCL/GDL interface. The mass transfer resistance in the GDL and the molar flux of oxygen are expressed as [17]

$$R_{GDL} = \frac{\delta_{GDL}}{D^{eff}_{O_2,GDL}} \tag{38}$$

$$N''_{O_2} = \frac{J}{4\mathscr{F}} \tag{39}$$

where $D^{eff}_{O_2,GDL}$ is the effective oxygen diffusivity in the GDL. Since the GDL consists of liquid-gas mixture, the effective diffusivity of oxygen is estimated using the following expression [37,38]:

$$D^{eff}_{O_2,GDL} = D_{O_2,g} - \frac{3\left(1-f_g\right)D_{O_2,g}}{\frac{3D_{O_2,g}}{D_{O_2,g}-D_{O_2-H_2O_{(\ell)}}} - \frac{3(1-f_\ell)D_{O_2-H_2O_{(\ell)}}}{f_\ell - 3\left(1-f_g\right)}} - f_g \tag{40}$$

where $D_{O_2,g}$ and $D_{O_2-H_2O_{(\ell)}}$ are the oxygen diffusion coefficients in the gas phase and liquid water in the GDL, respectively, and f_g and f_ℓ are the volume fractions of gas phase and liquid water in the GDL, respectively. It should be pointed out that summation of the volume fractions of liquid water, gas phase, and solid phase has to be unity in the GDL.

3.6. Activation overpotential in CCL

The activation overpotential in the CCL of a PEM fuel cell can be estimated from the following analytical formulation developed in our earlier study [17]:

$$\eta_{act} = \frac{\mathscr{R}T}{\alpha_c n\mathscr{F}} \cos h^{-1}\left[1 + \frac{J^2}{4\sigma^{eff}_m \left(\frac{\mathscr{R}T}{\alpha_c n\mathscr{F}}\right)(1-s_\ell)^q A_v J_0^{O_2}\left(\frac{C_{O_2,rs}}{C_{O_2,ref}}\right)}\right] \tag{41}$$

where σ^{eff}_m is the effective membrane conductivity in the CCL. It should also be noted that the above expression was derived by assuming identical transfer coefficients, i.e. $\alpha_c = \alpha_a$. The factor $(1 - s_\ell)$ in the denominator inside the square bracket is included here to account for the variation of active reaction

area with liquid saturation, where q is the order for the active area reduction due to the liquid saturation that is also known as saturation exponent.

The effective membrane conductivity in the CCL is estimated from the following expression [37,38]:

$$\sigma_m^{\text{eff}} = \sigma_m - \frac{3(1-f_m)\sigma_m}{3-f_m} - \frac{3f_v\left(\sigma_m - \frac{3(1-f_m)\sigma_m}{3-f_m}\right)}{2+f_v} \tag{42}$$

in which σ_m is the membrane conductivity, f_s, f_m, f_v are the volume fractions of solid platinum/carbon (Pt/C) particles, electrolyte membrane, and void space in the CCL, respectively. Here, the fraction of void space is simply the CCL porosity, while the volume fraction of membrane (usually Nafion) in the CCL can be related through the Nafion content %N (defined as the weight percentage of Nafion in the sum of Nafion and solid Pt/C particles) by [16,17]

$$f_m = \frac{\%N}{(1-\%N)\rho_m}\frac{m_{\text{Pt}}}{\%\text{Pt}\cdot\delta_{\text{CL}}} \tag{43}$$

where ρ_m is the density of Nafion, %Pt is the mass percentage of platinum in the combined total mass of Pt/C particles, m_{Pt} is the Pt-loading, and δ_{CL} is the catalyst layer thickness. If the catalyst layer surface area (A_{CL}) and carbon weight (W_C) are known, %Pt can be calculated from the following relation:

$$\%\text{Pt} = \frac{m_{\text{Pt}}A_{\text{CL}}}{m_{\text{Pt}}A_{\text{CL}} + W_C} \tag{44}$$

The volume fraction of solid Pt/C in the CCL is related to %Pt, catalyst layer thickness, and the densities of platinum and carbon black (ρ_{Pt} and ρ_C) as

$$f_s = \left(\frac{1}{\rho_{\text{Pt}}} + \frac{1-\%\text{Pt}}{\%\text{Pt}\cdot\rho_C}\right)\frac{m_{\text{Pt}}}{\delta_{\text{CL}}} \tag{45}$$

3.7. *Dimensionless liquid water profile*

Using the boundary condition at the GDL/CCL interface given in the previous section, the expressions for liquid water transport in the CCL become:

$$-0.541\left(s_\ell^7 - s_b^7\right) + 0.556\left(s_\ell^6 - s_b^6\right) - 0.193\left(s_\ell^5 - s_b^5\right) = \left(\bar{x}^2 - 1\right)\bar{R}_w + (\bar{x} - 1)\bar{R}_d \tag{46}$$

$$0.541\left(s_\ell^7 - s_b^7\right) - 0.707\left(s_\ell^6 - s_b^6\right) + 0.283\left(s_\ell^5 - s_b^5\right) = \left(\bar{x}^2 - 1\right)\bar{R}_w + (\bar{x} - 1)\bar{R}_d \tag{47}$$

where Eq. (46) is for the hydrophilic CCL and Eq. (47) is for the hydrophobic CCL. Here s_b is the liquid saturation at the GDL/CCL interface that can be obtained from Eqs. (33) and (34) for hydrophobic and hydrophilic CCLs, respectively, $\bar{x}$ is the dimensionless distance along the catalyst layer thickness, $\bar{R}_w$ is the dimensionless water production in the CCL from the electrochemical reaction and condensation, and $\bar{R}_d$ is the dimensionless net water transport from the membrane to the CCL by the electro-osmotic drag and back-diffusion. The dimensionless distance along the CCL thickness is defined as

$$\bar{x} = \frac{x}{\delta_{\text{CL}}} \tag{48}$$

where δ_{CL} is the catalyst layer thickness.

The dimensionless water production in the CCL from the electrochemical reaction and condensation is defined by the following expression:

$$\bar{R}_w = \frac{0.5\mu_\ell\delta_{\text{CL}}^2}{\epsilon(\epsilon K)^{0.5}\gamma\cos\theta_c}\left[\frac{2\hat{M}_{H_2O}A_v\mathscr{R}_{c,\text{red}}}{\rho_\ell} + k_c\frac{\epsilon x_g^{H_2O}\hat{M}_{H_2O}}{\rho_\ell\mathscr{R}T}\left(x_g^{H_2O}\langle P_g\rangle^g - P_{\text{sat}}\right)\right] = \text{CDT}\left[(\text{EPT})^{-1} + (\text{PCT})^{-1}\right] = \Pi_1 + \Pi_2 \tag{49}$$

where Π_1 and Π_2 are the dimensionless numbers that are named as the "*dimensionless time of first kind*" and "*dimensionless time of second kind*", respectively. The dimensionless time of first kind represents the ratio between the capillary diffusion time (CDT) to the electrochemical production time (EPT) and the dimensionless time of second kind represents the ratio between the capillary diffusion time to the phase change time (PCT) at steady-state. Conversely, the term $\bar{R}_d$ is defined as

$$\bar{R}_d = \frac{0.5\mu_\ell\delta_{\text{CL}}^2}{\epsilon(\epsilon K)^{0.5}\gamma\cos\theta_c}\left[\frac{2\alpha J\hat{M}_{H_2O}}{\rho_\ell\delta_{\text{CL}}\mathscr{F}}\right] = \Pi_3 \tag{50}$$

where Π_3 is the "*dimensionless time of third kind*", which represents the ratio between the capillary diffusion time to the time required for liquid water transport by the net electro-osmotic drag and back-diffusion processes across the CCL. These dimensionless time constants will provide insight about how much liquid water would be accumulated in the CCL and transported from the CCL to the gas flow channel through the GDL. Since the capillary diffusion is the major mode of water transport from the CCL to the GDL, the higher the time constants are, the higher the liquid water accumulation. Hence, the water saturation will also be higher in the CCL for higher time constant values.

4. Results and discussion

In the following subsections, the results are presented for both hydrophilic and hydrophobic CCLs that are estimated using the analytical solutions of liquid water transport given in Eqs. (46) and (47). The analytical expressions for the liquid water distribution, however, require several physical and electrochemical parameters as well as liquid water saturation at the GDL/CCL interface, oxygen concentration at the reaction site, and cathode activation overpotential. The required physical electrochemical parameters are listed in Table 2, while the analytical expressions are already provided in previous sections for liquid water saturation at the GDL/CCL interface, oxygen concentration at the reaction site, and cathode activation overpotential, respectively. It is worthwhile to note that the proposed analytical expressions for liquid water distribution in the CCL do not involve any complicated numerical modeling or solutions to several simultaneous transport equations except the expressions given in Sections (3.4)–(3.6).

4.1. *Liquid saturation profile in cathode catalyst layer*

The liquid saturation profiles obtained from the 1D analytical solution of liquid water transport in the CCL of a PEM fuel cell

Table 1 – Electrochemical and transport properties used in Ref. [21].

Description	Value
Cell temperature (K)	353
Faraday constant (C mol^{-1})	96 487
Liquid water density (kg m^{-3})	971.8
Liquid water viscosity (Pa s)	3.56×10^{-4}
Surface tension (N m^{-1})	0.0625
GDL porosity	0.5
GDL permeability (m^2)	6.875×10^{-13}
GDL thickness (m)	300×10^{-6}

are shown in Fig. 3 for two different current densities as indicated in the figure. Both hydrophobic and hydrophilic cases are considered, where the solid lines represent the profile in a CCL having contact angle of 80° and the dashed lines depict the profile for contact angle of 100° for the case when the electro-osmotic drag is significant than the back-diffusion at the membrane/CCL interface. As observed from Fig. 3, the hydrophilic CCL shows higher liquid saturation than the hydrophobic CCL. It should be pointed out that for both cases, the GDL is considered as hydrophobic with a contact angle of 100°. The GDL properties are identical of Ref. [21] that are listed in Table 1. In Fig. 3, the higher liquid saturation level near the membrane/CCL interface for a hydrophilic CCL than a hydrophobic CCL suggests slower liquid water transport from the CCL to the GDL if the catalyst layer is hydrophilic. This situation might be favorable for the proton transport in the CCL. At the same time, the higher liquid saturation at the membrane/CCL interface also implies that the higher level of water transport from the membrane to the CCL that might eventually dry out membrane. Further, the higher level of liquid accumulation in the CCL, particularly in a hydrophilic CCL, will require a better water management in the GDL.

Table 2 – Parameters used in the model calculations.

Description	Value	Source
Gas pressure (atm)	3	
Relative humidity (%)	100	
Gas constant (J mol^{-1} K^{-1})	8.315	
Cell width (mm)	70.7	[17]
Cell height (mm)	70.7	[17]
Flow channel width (mm)	1	[21]
Flow channel height (mm)	1	[21]
Liquid saturation in gas channel	0	[21]
Catalyst layer thickness (m)	20×10^{-6}	[17]
Anodic and cathodic transfer coefficients	0.5	[16]
Reference oxygen concentration (mol m^{-3})	1.2	[16]
GDL contact angle (°)	100	[21]
Drag coefficient, α	0.25	[15]
Condensation rate constant (s^{-1})	100	[15]
Platinum loading (mg cm^{-2})	0.3	[17]
%Wt of Platinum	0.2	[17]
%Wt of Nafion	0.3	[17]
Catalyst surface area per unit mass of catalyst (m^2 gm^{-1})	112	[17]
Membrane conductivity (S m^{-1})	17	[15]
Platinum density (kg m^{-3})	21.5×10^3	[15]
Carbon density (kg m^{-3})	2.0×10^3	[15]
Nafion density (kg m^{-3})	1.9×10^3	[15]

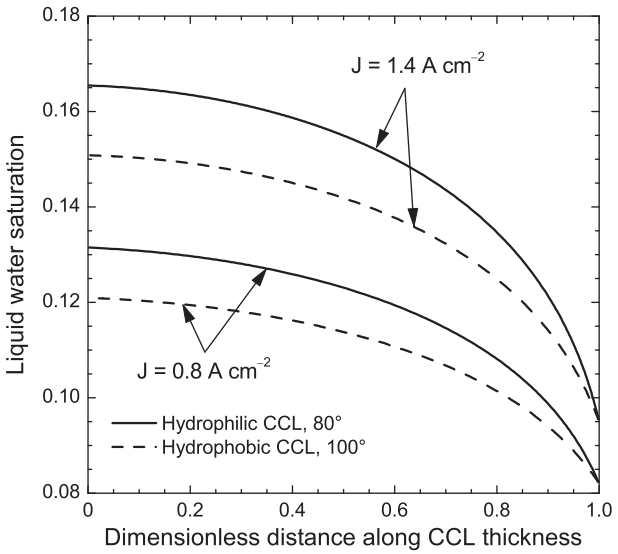

Fig. 3 – Liquid saturation profile across the CCL of a PEM fuel cell predicted by 1D analytical model for two different current densities as indicated in the legend. The solid and dashed lines represent liquid water profile for the CCL having contact angles of 80° and 100°, respectively.

4.2. *Effect of surface wettability*

Fig. 4 depicts the effect of contact angle on the liquid water distribution in the CCL for a current density of 0.8 A cm^{-2}. All the parameters are identical to those for Fig. 3, except the CCL contact angles that are indicated in the legend. It is observed that the contact angles have significant influence on the liquid water distribution inside a fuel cell catalyst layer. In a hydrophilic catalyst layer ($\theta_c < 90°$) as shown in Fig. 4a, the CCL having a contact angle of 89° shows significantly higher liquid saturation than the CCL having lower contact angle or higher wettability. It is mainly due to the capillary pressure. Since the capillary pressure drives the flow of liquid water in the CCL and the capillary pressure reduces significantly with contact angle, the hydrophilic CCL with high contact angle shows higher liquid saturation. Conversely, in a hydrophobic catalyst layer ($\theta_c > 90°$) as shown in Fig. 4b, lower contact angle shows a higher liquid saturation. As the hydrophobicity increases, the liquid saturation in the catalyst layer decreases rapidly. This result also implies that a hydrophobic catalyst layer would enhance water transport from the catalyst layer, whereas a catalyst layer has to be hydrophilic in nature for better proton transport. Hence, a balance between the hydrophlicity and hydrophobicity might be desirable for a PEM fuel cell catalyst layer for better water transport as well as higher cell performance.

The reason why a lower contact angle or highly hydrophilic CCL (Fig. 4a) shows low liquid saturation can be justified if we

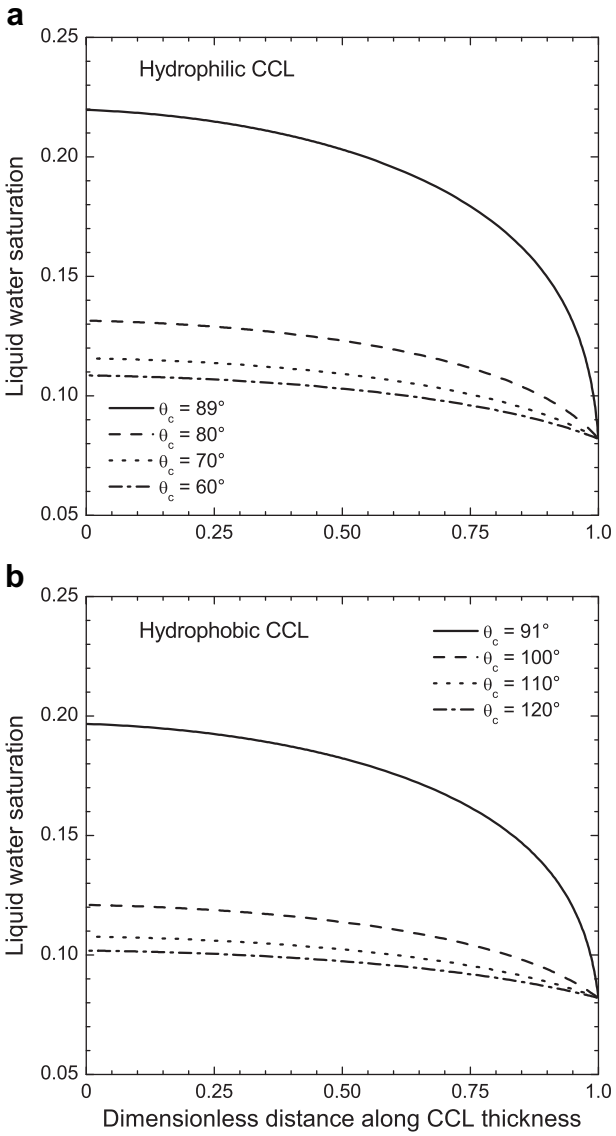

Fig. 4 – Liquid saturation profile across the dimensionless distance along CCL thickness predicted by 1D analytical model of liquid water transport for different contact angles.

notice the experimental measurements of the functional dependence of capillary pressure on the liquid saturation that is provided by Ustohal et al. [39] for a porous media with hydrophilic pore wettability for an air-water system. It has been observed that the liquid saturation decreases for an air-water system with the increases of wettability of the medium or the pressure difference between the phases [39]. Hence, the results presented in Fig. 4 are consistent with what Ustohal et al. [39] observed experimentally. The results in Fig. 4 also show that the liquid saturation for hydrophilic CCL could be as high as 22% at the membrane/CCL interface and about 20% for hydrophobic CCL, even for the case of no liquid saturation in the gas channel and with a hydrophobic GDL. In other words, the liquid water transport will be significantly reduced due to the lower hydrophilicity of a hydrophilic CCL. Whereas highly hydrophilic CCL (low contact angle) shows lowest liquid saturation, hence better water transport from the CCL to the GDL. Therefore, this study reveals that the higher wettability increases the water transport from a hydrophilic CCL and will reduce the liquid saturation. Therefore, a highly hydrophilic CCL would be quite capable of keeping the reaction site wet enough for favorable electrochemical reaction and proton transport even with low liquid saturation due to the higher surface wettability. Practically, the liquid water saturation at the GDL/flow channel interface is higher than zero, hence, the water saturation at the membrane/CCL interface could be significantly higher than the values observed in Fig. 4. The trends observed in Fig. 4 seem to remain similar even for a higher saturation at the GDL/flow channel interface.

The common perception that a highly hydrophilic surface means higher liquid saturation seems not correct. A highly hydrophilic surface represents high wettability, and due to high wettability, less amount of liquid water is required to wet a surface than the amount of water required to wet the same amount of low-hydrophilic surface. In highly hydrophilic pores, the volume of liquid water will be less compared to the liquid water volume in low-hydrophilic pores that will eventually provide less water saturation for low contact angles and high wettability. This phenomenon can be further explained by considering a liquid droplet over a solid surface and changing its contact angle as shown in Fig. 5. Here, the four subfigures show how the volume of liquid water over a surface changes with contact angles. The top-left figure represents the hydrophobic case and other three figures depict the hydrophilic cases. Although the hydrophobic and hydrophilic cases have the same liquid volume over the solid surface (except the bottom-right figure), the surface wettability becomes higher for the hydrophilic cases. The top-right figure represents a hydrophilic case with higher contact angle when the liquid phase did not wet the surface completely. The bottom-left figure represents the intermediate contact angle case but the liquid phase completely wets the solid surface (surface 1). For both cases, the liquid phase volume over the solid surface is the same. Considering a further lower value of contact angle than the bottom-left figure, as shown in bottom-right part, eventually reveals that the liquid phase is drained out from the solid surface due to the lower contact angle or higher hydrophilicity.

Recalling the definition of capillary pressure in the porous CCL, we can immediately recognize that the lower contact angles also represent higher capillary pressures. Since the

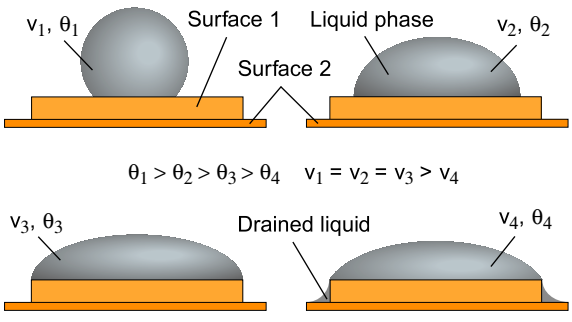

Fig. 5 – Effect of contact angles on the liquid phase volume over a solid surface.

capillary pressure is the gas phase pressure minus the liquid phase pressure for a hydrophilic medium, the liquid phase pressure will decrease with the capillary pressures. Hence, the gas phase will push away the liquid phase from a hydrophilic pore, and eventually reduces the volume of liquid water over the solid phase. Conversely, the reaction site needs to be well hydrated for better electrochemical reaction that can even be achieved with less liquid water if the surface wettability is higher. A balance of liquid saturation and surface wettability is desirable as the high liquid saturation may block pores that will eventually hinder the oxygen transport to the reaction site, while the low liquid saturation may cause dry out of the reaction site and membrane that will hinder the proton transport to the reaction site.

4.3. *Effect of electro-osmotic drag and back-diffusion*

The significance of water transport from the anode side to the cathode side of a PEM fuel cell due to the electro-osmotic drag and its effect on the catalyst layer liquid saturation are also investigated. Fig. 6 shows the liquid saturation profile across the CCL thickness predicted by 1D analytical model for several electro-osmotic drag coefficients as indicated in the legend. Here, the liquid saturations are estimated in a CCL having a contact angle of 80° for a current density of 0.8 A cm^{-2}. All other parameters are identical to those for Figs. 3 and 4. The level of liquid saturation increases when the electro-osmotic transport is higher than the water transport by back-diffusion ($\alpha > 0$), while the higher back-diffusion ($\alpha < 0$) causes the reduction of liquid saturation in the CCL. To be specific, the liquid saturation would be increased by about 5% at the membrane/CCL interface for the most widely used electro-osmotic drag coefficient ($\alpha = 0.25$) compared to when a balance exists between water transport by the electro-osmotic drag and the back-diffusion process ($\alpha = 0$). Although

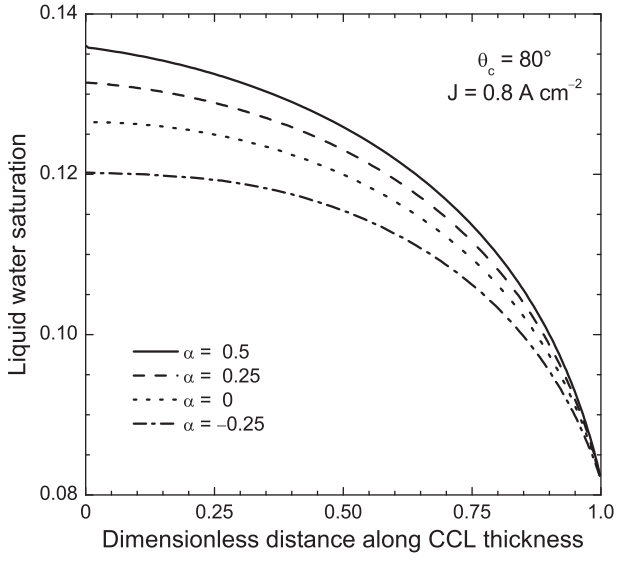

Fig. 6 – Effect of the electro-osmotic drag and back-diffusion on liquid saturation profile across the CCL thickness predicted by 1D analytical model of liquid water transport.

the variations observed in Fig. 6 is much lower than the variations observed in Fig. 4 for different contact angles, nonetheless, the significance of water transport from the anode to the cathode side of a PEM fuel cell due to electro-osmotic drag is crucial for proper water balance in the CCL. For instance, the total variation observed at the membrane interface is about 13% while varying the electro-osmotic drag coefficients from −0.25 to 0.5 that seems significant to reduce the performance of a PEM fuel cell.

4.4. *Effect of flooding on performance*

It has been widely investigated how the performance of a PEM fuel cell degrades due to the liquid water flooding in the GDL [12,15,21]. Flooding in the GDL hinders oxygen transport, whereas flooding in the CCL not only hinders oxygen transport but also reduces fuel cell performance by covering electrochemically active site with liquid water. Therefore, flooding seems to be more sensitive to the CCL than the GDL resistance to oxygen transport. Since most of the electrochemical reaction occurs near the membrane/CCL interface, the effect of water flooding in the CCL has been investigated by assuming a uniform liquid saturation that is approximately equal to the liquid saturation observed near the membrane/CCL interface.

Fig. 7 depicts the activation overpotentials as a function of current density for five different liquid saturations at the CCL as indicated in the legend. Here, four parts of Fig. 7 represent four cases of the active area reduction by liquid saturation, namely, $q = 1$, 2, 5, and 8. In these results, the resistance to oxygen transport to the CCL includes both the GDL and CCL resistances. The CCL resistance to the oxygen transport is estimated using an identical formulation given for the GDL resistance in Section 3.5, while the effective oxygen diffusivity in the CCL is estimated using the formulation developed in Ref. [38]. Surprisingly, the effect of water flooding on the cathode activation overpotential shown in Fig. 7a for the case of linear reduction ($q = 1$) of active reaction area by liquid saturation does not show significant variation. Clearly, with 50% liquid saturation, the activation overpotential only increases by about 5% compared to the activation overpotential estimated for 10% liquid saturation at 0.8 A cm^{-2}. However, it has been observed in literature of high cathode overpotential due to GDL water flooding [21], which includes activation, ohmic, and concentration overpotential together. Here, we have only shown the activation loss at the CCL. It seems that there might be a threshold limit for the cathode activation overpotential in the CCL, which is less sensitive to the liquid saturation when a linear reduction of active reaction area with liquid saturation is considered. Even for the quadratic reduction of active reaction site with liquid saturation shows only a small variation in the activation potential in catalyst layer as shown in Fig. 7b. For the higher order reduction of active reaction area (Fig. 7c and d), the liquid saturation shows significant effect on the cathode activation potential. For instance, activation overpotential at the cathode cathode catalyst layer would be 34% higher at a current density of 1.0 A cm^{-2} when the liquid saturation increases from 0.1 to 0.5 as observed in Fig. 7d.

Clearly, the approximation of linear reduction of active reaction area due to the liquid saturation might not be a good

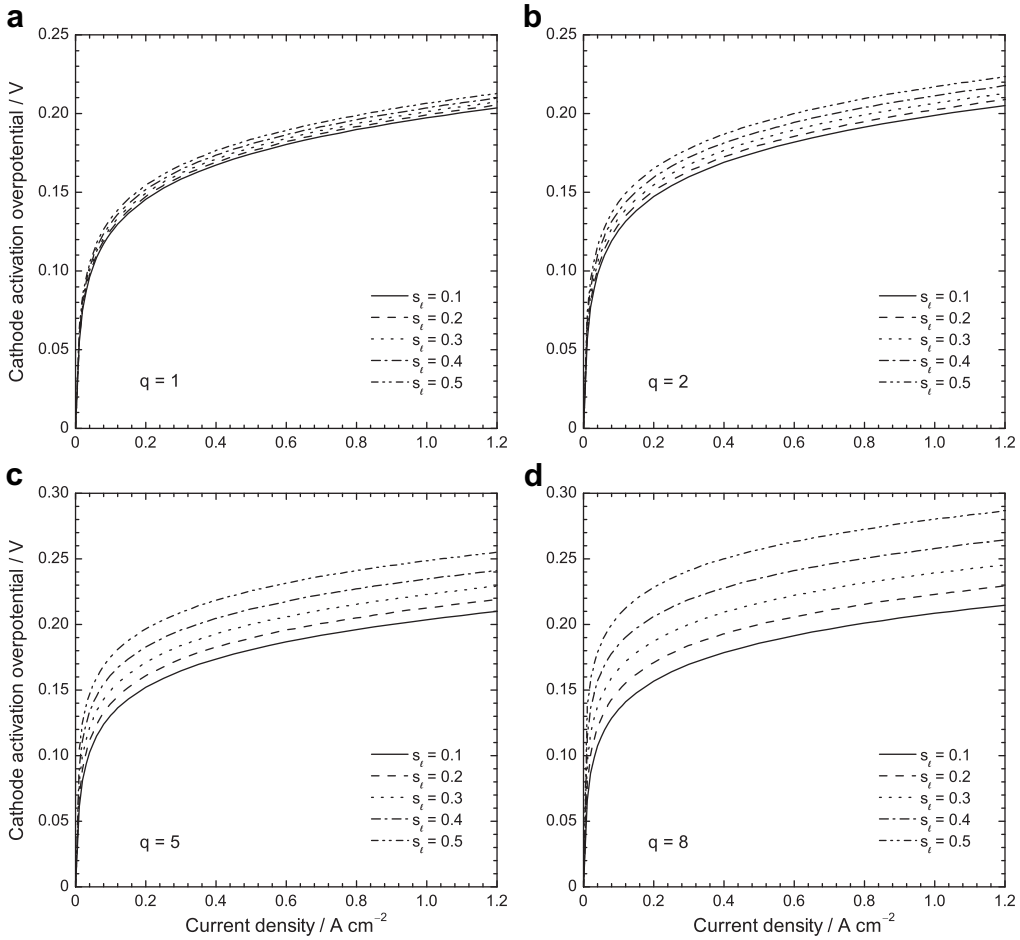

Fig. 7 – Effect of liquid saturation on the cathode activation overpotential of a PEM fuel cell for a current density of 0.8 A cm^{-2} for different values of saturation exponent, *q*, as indicated in the legend.

approximation. Since the catalyst particle has high surface area to volume ratio, the linear reduction of reaction surface area with the liquid water volume in the CCL would always overestimate the active reaction area and underestimate the effect of water flooding on the cell potential. It is worthwhile to note that the resistance to the oxygen transport has been estimated using a linear approximation. If a pore in the GDL is completely blocked by liquid water, then oxygen needs to be dissolved to the liquid water before continuing to diffuse that will encounter higher resistance to the transport process compared to the resistance estimated considering a diffusion mechanism only. Nonetheless, the results presented in Fig. 7 show that the liquid saturation will eventually reduce the fuel cell performance and a higher order approximation for the active area reduction should be considered.

4.5. *Effect of time constants*

The effects of the dimensionless time constants on the liquid saturation are investigated in this section. Fig. 8 shows the variation of liquid water saturation in the CCL of a PEM fuel cell with different values of "dimensionless time of first kind" as indicated in the legend for a current density of 0.8 A cm^{-2}. Since the dimensionless time of first kind (Π_1) depends on several geometrical and physical properties of the CCL that will eventually affect the other time constants, the dimensionless time of second kind (Π_2) and third kind (Π_3) were kept constant while investigating the effect of the dimensionless time of first kind. The dimensionless time of second kind (Π_2) and third kind (Π_3) were estimated with the parameter values listed in Tables 1 and 2. As expected, for the higher values of time constant, the liquid saturation becomes very high in the CCL. Physically, the higher values of Π_1 represent the slower capillary diffusion process or the faster electrochemical production. The maximum liquid saturation in a two-phase situation, which is physically possible to reach in the CCL, is shown by the uppermost curve when $\Pi_1 = 1$. The dimensionless time of first kind of unity means the time requires to produce 1 unit of liquid water and the time requires to diffuse the same amount of liquid water across the CCL by the capillary diffusion process are the same at that maximum saturation level for a steady-state condition. In other words, the moment the liquid water generated in the CCL, it will be instantly diffused away to the GDL or to the membrane. The liquid water will not be able to occupy further volume in the porous catalyst layer than the saturation shown for $\Pi_1 = 1$ due to the presence of gas phase. Theoretically, the time constant can be higher than unity. At the values higher than unity,

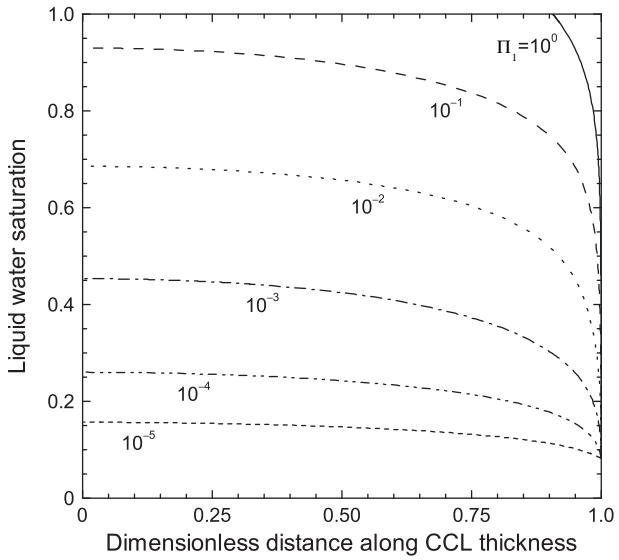

Fig. 8 – Effect of dimensionless time constant, Π_1, on liquid saturation in the CCL of a PEM fuel cell for a current density of 0.8 A cm^{-2}. Each line represents different values of the "dimensionless time of first kind" as indicated in the legend.

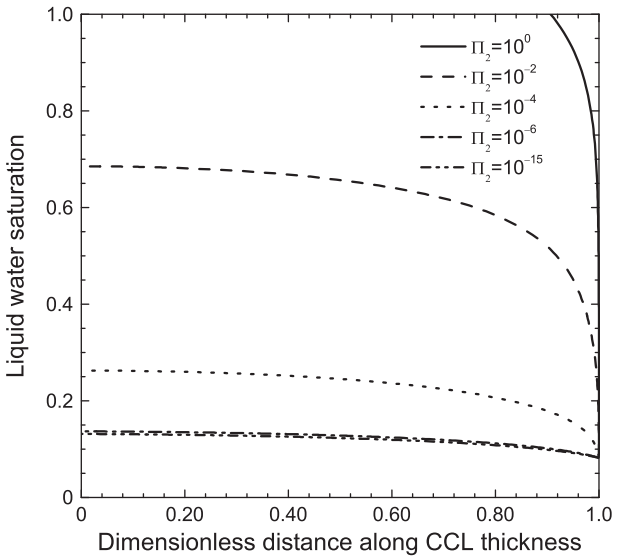

Fig. 9 – Variation of liquid saturation in the CCL of a PEM fuel cell with the "dimensionless time of second kind" for a current density of 0.8 A cm^{-2}.

however, the entire CCL will be flooded with liquid water that might eventually stop the electrochemical reaction, hence the fuel cell operation, as there will be no gas phase present in the CCL. In such case, the entire two-phase process will be transformed into a single-phase process, hence the two-phase formulation proposed in this study will not be valid for $\Pi_1 > 1$. Conversely, the liquid saturation will be close to zero when the dimensionless time constant goes to an infinitely small value. However, for a steady fuel cell operation, liquid water has to be present in the CCL. It is always desirable to have a certain liquid saturation that will provide a stable liquid film over the catalyst surface for better proton transport. Even with a high surface wettability, the liquid film can be unstable if the liquid saturation is low due to insufficient liquid water. The discontinuous liquid film or low liquid saturation will then hinder the proton transport, hence reduces the cell performance. Therefore, the lowest possible time constant can be in the order of 10^{-5} as observed from Fig. 8 if we assume the CCL has modest wettability.

Fig. 9 depicts the variation of liquid saturation in the CCL of a PEM fuel cell for the second dimensionless time constant, Π_2 (ratio between capillary diffusion time to phase change time). Here, the dimensionless time of first kind (Π_1) and third kind (Π_3) were estimated with the parameter values listed in Tables 1 and 2, and kept constant while varying the second dimensionless time constant. Similar to Π_1, the liquid saturation profile for the second time constant also shows similar trend. However, the order of magnitude is found to be very small compared to the first time constant. For instance, it has been estimated to be in the order of 10^{-14} for the parameter values listed in Tables 1 and 2, while the order for the first time constant is about 10^{-5}. As observed from Fig. 9 at the practical range ($\Pi_2 \approx 10^{-14}$), the effect of dimensionless time of second kind on the liquid saturation in the CCL is negligible compared to the contribution of liquid saturation from the electrochemical process (comparing $\Pi_2 = 10^{-10}$ and 10^{-15}). Physically, the higher values of second time constant represent slower capillary diffusion or faster phase change process. Therefore, the results shown in Fig. 9 further imply that the capillary diffusion process is much faster than the liquid water production from a condensation process.

For the "dimensionless time of third kind", the results are shown in Fig. 10 for a current density of 0.8 A cm^{-2}. Here, the variation of liquid saturation across the CCL thickness are shown for several values of third time constant as indicated in the legend, while the dimensionless time of first kind (Π_1) and second kind (Π_2) were kept constant. Since the order of magnitude for the dimensionless time of third kind is found to be 10^{-5} using the parameters listed in Tables 1 and 2, the

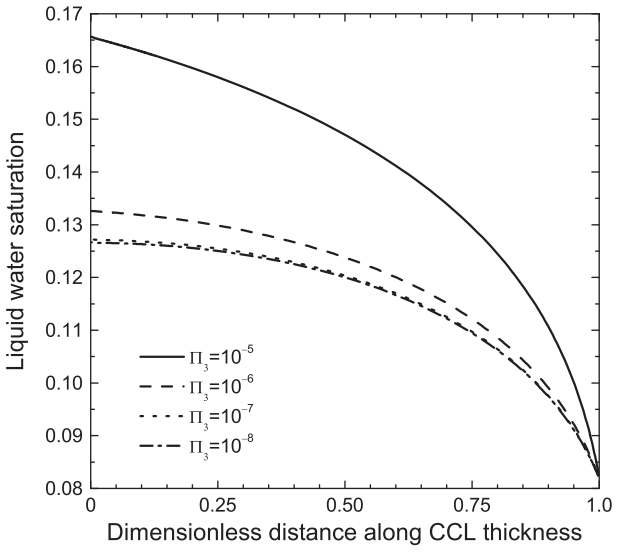

Fig. 10 – Variation of liquid saturation in the CCL of a PEM fuel cell with the "dimensionless time of third kind" for a current density of 0.8 A cm^{-2}.

result for the dimensionless time of third kind are presented only for the values lower than or equal to 10^{-5}. The liquid saturation profiles across the CCL thickness are found to be almost independent of the time constant for lower values of Π_3. This is mainly due to the fact that the time requires for water transport across the CCL by the capillary diffusion. Physically, the higher values of third time constant represent a slower capillary diffusion or a faster electro-osmotic drag and back-diffusion process. Therefore, the time requires for liquid water transport by the capillary diffusion is small compared to the time requires for the electro-osmotic drag and back-diffusion process at smaller Π_3. It should be pointed out that for the practical range of third time constant, 10^{-5}–10^{-6}, the effect of the third time constant on the liquid saturation in CCL is significant. Hence, the electro-osmotic drag and back-diffusion process should always be considered during the water management for PEM fuel cells.

5. Conclusions

A simplified mathematical formulation of liquid water transport in the CCL of a PEM fuel cell has been developed and the one-dimensional analytical solutions have been provided for both the hydrophilic and hydrophobic CCLs. It has been observed that the wetting properties of a CCL control the flooding behavior, and hydrophilic characteristic of CCL plays significant role on the cell performance. Although a hydrophobic CCL has shown less liquid saturation compared to a hydrophilic CCL at the similar hydrophobicities or hydrophilicities, it seems possible to reduce liquid saturation by increasing the surface wettability (i.e. lowering the contact angle) of a hydrophilic CCL. At the same time, high surface wettability of hydrophilic CCL would provide sufficient surface wetting to enhance proton transport in the CCL. Based on the analysis of the dimensionless time constants, it is found that liquid water production from the phase change process is almost negligible compared to liquid water production from the electrochemical process. However, the liquid water transport by the electro-osmotic drag and back-diffusion from the membrane to the CCL has significant contribution to the liquid accumulation, hence it cannot be neglected. The effect of water flooding on the activation overpotential is found to be less sensitive if a linear reduction of active reaction area is assumed, whereas the higher order reduction of active reaction area shows significant increase of activation overpotential due to the liquid saturation. Hence, the widely used linear approximation of the reduction of active reaction site due to the liquid water saturation seems to be an underestimation. The dimensionless time constants defined in this study might be a useful tool in investigating other flows in porous medium, such as ground water transport, oil transport in oil sands, and membrane filtration.

Acknowledgments

The financial support of the Natural Sciences and Engineering Research Council of Canada is gratefully acknowledged. P.K.D. also thanks the National Research Council of Canada, the Ontario Graduate Scholarship program, and the University of Waterloo for postgraduate scholarships.

Nomenclature

A	interfacial mass-transfer rate (kg m^{-3} s^{-1} Pa^{-1})
A_s	catalyst surface area per unit mass of catalyst (m^2 kg^{-1})
A_v	reactive surface area per unit volume (m^{-1})
C	integration constant
C_{O_2}	oxygen concentration (mol m^{-3})
d_h	hydraulic diameter (m)
D	diffusivity (m^2 s^{-1})
f	volume fraction
$\mathscr{F}$	Faraday's constant (C mol^{-1})
J	current density (A cm^{-2})
k_c	condensation rate constant (s^{-1})
k_v	evaporation rate constant (Pa^{-1} s^{-1})
k_{rl}	relative permeability (m^2)
$\hat{M}$	molecular weight (kg mol^{-1})
P	pressure (Pa)
P_c	capillary pressure (Pa)
P_{sat}	saturation pressure (Pa)
$\mathscr{R}$	universal gas constant (J mol^{-1} K^{-1})
s	saturation
T	temperature (K)
u	velocity (m s^{-1})
x_{H_2O}	water mole fraction
x_{N_2}	nitrogen mole fraction
x_{O_2}	oxygen mole fraction

Greek letters

α	drag coefficient
α_a	anodic transfer coefficient
α_c	cathodic transfer coefficient
γ	surface tension (N m^{-1})
Γ	source term
δ	thickness (m)
ϵ	porosity
η_c	activation overpotential (V)
θ_c	contact angle
μ	viscosity (Pa s)
ν	kinematic viscosity (m^2 s^{-1})
ρ	density (kg m^{-3})
σ	conductivity (S m^{-1})

Subscripts & superscripts

b	boundary value
C	carbon
CL	catalyst layer
eff	effective value
g	gas phase
GDL	gas diffusion layer
ℓ	liquid phase
m	membrane phase
Pt	platinum
ref	reference value
s	solid phase
v	void space

Abbreviations

CCL	cathode catalyst layer
GDL	gas diffusion layer
PEM	polymer electrolyte membrane

REFERENCES

[1] Li X. Principles of fuel cells. New York: Taylor & Francis; 2006.
[2] Bernardi D, Verbrugge M. Mathematical model of a gas-diffusion electrode bonded to a polymer electrolyte. AIChE J 1991;37:1151–63.
[3] Springer T, Zawodzinski T, Gottesfeld S. Polymer electrolyte fuel cell model. J Electrochem Soc 1991;138:2334–42.
[4] Fuller T, Newman J. Water and thermal management in solid-polymer-electrolyte fuel cells. J Electrochem Soc 1993; 140:1218–25.
[5] Yamada H, Hatanaka T, Murata H, Morimoto Y. Measurement of flooding in gas diffusion layers of polymer electrolyte fuel cells with conventional flow field. J Electrochem Soc 2006;153:A1748–54.
[6] Ho Jung U, Uk Jeong S, Tae Park K, Mee Lee H, Chun K, Woong Choi D, et al. Improvement of water management in air-breathing and air-blowing PEMFC at low temperature using hydrophilic silica nano-particles. Int J Hydrogen Energy 2007; 32:4459–65.
[7] Liu X, Guo H, Ye F, Ma C. Flow dynamic characteristics in flow field of proton exchange membrane fuel cells. Int J Hydrogen Energy 2008;33:1040–51.
[8] Owejan J, Gagliardo J, Sergi J, Kandlikar S, Trabold T. Water management studies in PEM fuel cells, part I: fuel cell design and in situ water distributions. Int J Hydrogen Energy 2009; 34:3436–44.
[9] Lu Z, Kandlikar S, Rath C, Grimm M, Domigan W, White A, et al. Water management studies in pem fuel cells, part II: ex-situ investigation of flow maldistribution, pressure drop and two-phase flow pattern in gas channels. Int J Hydrogen Energy 2009;34:3445–56.
[10] Janssen GJM. A phenomenological model of water transport in a proton exchange membrane fuel cell. J Electrochem Soc 2001;148:A1313–23.
[11] You L, Liu H. A parametric study of the cathode catalyst layer of PEM fuel cells using a pseudo-homogeneous model. Int J Hydrogen Energy 2001;26:991–9.
[12] Natarajan D, Nguyen T. Three-dimensional effects of liquid water flooding in the cathode of a PEM fuel cell. J Power Sources 2003;115:66–80.
[13] Sahraoui M, Kharrat C, Halouani K. Two-dimensional modeling of electrochemical and transport phenomena in the porous structures of a PEMFC. Int J Hydrogen Energy 2009;34:3091–103.
[14] Pasaogullari U, Wang C. Two-phase modeling and flooding prediction of polymer electrolyte fuel cells. J Electrochem Soc 2005;152:A380–90.
[15] Song D, Wang Q, Liu ZS, Huang C. Transient analysis for the cathode gas diffusion layer of PEM fuel cells. J Power Sources 2006;159:928–42.
[16] Das PK, Li X, Liu ZS. A three-dimensional agglomerate model for the cathode catalyst layer in PEM fuel cells. J Power Sources 2008;179:186–99.
[17] Das PK, Li X, Liu ZS. Analytical approach to polymer electrolyte membrane fuel cell performance and optimization. J Electroanal Chem 2007;604:72–90.
[18] Trabold T, Owejan J, Jacobson D, Arif M, Huffman P. In situ investigation of water transport in an operating PEM fuel cell using neutron radiography: part 1 – experimental method and serpentine flow field results. Int J Heat Mass Transf 2006; 49:4712–20.
[19] Owejan J, Trabold T, Jacobson D, Arif M, Kandlikar S. Effects of flow field and diffusion layer properties on water accumulation in a PEM fuel cell. Int J Hydrogen Energy 2007; 32:4489–502.
[20] Ous T, Arcoumanis C. The formation of water droplets in an air-breathing PEMFC. Int J Hydrogen Energy 2009;34: 3476–87.
[21] Pasaogullari U, Wang C. Liquid water transport in gas diffusion layer of polymer electrolyte fuel cells. J Electrochem Soc 2004;151:A399–406.
[22] Feindel K, LaRocque L, Starke D, Bergens S, Wasylishen R. In situ observations of water production and distribution in an operating H_2/O_2 PEM fuel cell assembly using ^1H NMR microscopy. J Am Chem Soc 2004;126:11436–7.
[23] Park J, Li X, Tran D, Abdel-Baset T, Hussey D, Jacobson D, et al. Neutron imaging investigation of liquid water distribution in and the performance of a PEM fuel cell. Int J Hydrogen Energy 2008;33:3373–84.
[24] Neild D, Bejan A. Convection in porous media. New York: Springer; 1999.
[25] Berning T, Djilali N. A 3D, multiphase, multicomponent model of the cathode and anode of a PEM fuel cell. J Electrochem Soc 2003;150:A1589–98.
[26] Wang C. A fixed-grid numerical algorithm for two-phase flow and heat transfer in porous media. Numer Heat Transf Part B 1997;32:85–105.
[27] Leverett M. Capillary behavior in porous solids. Trans AIME 1941;142:152–69.
[28] Udell K. Heat transfer in porous media considering phase change and capillarity - the heat pipe effect. Int J Heat Mass Transf 1985;28:485–95.
[29] Natarajan D, Nguyen T. A two-dimensional, two-phase, multicomponent, transient model for the cathode of a proton exchange membrane fuel cell using conventional gas distributors. J Electrochem Soc 2001;148:A1324–35.
[30] Pisani L, Murgia G, Valentini M, D'Aguanno B. A working model of polymer electrolyte fuel cells - comparisons between theory and experiments. J Electrochem Soc 2002; 149:A898–904.
[31] Weber A, Darling R, Newman J. Modeling two-phase behavior in PEFCs. J Electrochem Soc 2004;151:A1715–27.
[32] Parthasarathy A, Srinivasan S, Appleby A, Martin C. Temperature-dependence of the electrode-kinetics of oxygen reduction at the platinum nafion interface-A microelectrode investigation. J Electrochem Soc 1992;139:2530–7.
[33] Birgersson E, Noponen M, Vynnyckya M. Analysis of a two-phase non-isothermal model for a PEFC. J Electrochem Soc 2005;152:A1021–34.
[34] Park Y, Caton J. An experimental investigation of electro-osmotic drag coefficients in a polymer electrolyte membrane fuel cell. Int J Hydrogen Energy 2008;33:7513–20.
[35] Perry R, Green D. Perry's chemical engineers' handbook. New York: McGraw-Hill; 1997.
[36] Bird R, Stewart W, Lightfoot E. Transport phenomena. New York: John Wiley & Sons Inc.; 1960.
[37] Das PK, Li X, Liu ZS. Estimation of effective transport properties for PEM fuel cells. In: Proceedings of the 4th International green energy Conference. Beijing, 2008. pp. 164–174. Paper ID 68.
[38] Das PK, Li X, Liu ZS. Effective transport coefficients in PEM fuel cell catalyst and gas diffusion layers: beyond Bruggeman approximation. Appl Energy, in press.
[39] Ustohal P, Stauffer F, Dracos T. Measurement and modeling of hydraulic characteristics of unsaturated porous media with mixed wettability. J Contam Hydrol 1998;33:5–37.